DOI: https://dx.doi.org/10.4314/gjpas.v28i1.6

GLOBAL JOURNAL OF PURE AND APPLIED SCIENCES VOL. 28, 2022: 39-50
COPYRIGHT© BACHUDO SCIENCE CO. LTD PRINTED IN NIGERIA ISSN 1118-0579
www.globaljournalseries.com, Email: globaljournalseries@gmail.com

SYNTHESIS, SPECTROSCOPIC, AND DENSITY FUNCTIONAL THEORY STUDIES OF THE CORROSION INHIBITIVE BEHAVIOUR OF *N*-(1,4-DIHYDRO-1,4-DIOXONAPHTHALENE-3-YL)PYRAZINE-2-CARBOXAMIDE CHELATOR-LIGAND

FESTUS CHIOMA, ODOZI, NNENNA W., AND MCHIHI M. MOSES, OLATUNDE, M. ABIMBOLA

(Received 2 December 2021; Revision Accepted 21 January 2022)

ABSTRACT

The inhibitory effect of *N*-(1,4-dihydro-1,4-dioxonaphthalene-3-yl) pyrazine-2-carboxamide (HL chelator) on the corrosion of mild steel (Ms) in 1M HCl remained appraised via weight loss (WL) estimations, atomic absorption spectrophotometer (AAS), scanning electron microscope (SEM) and computational studies. The adsorption of the appraised ligand remained found to conform to Langmuir adsorption isotherm (LAI). The data acquired for ΔG_{ads} denotes chemisorption adsorption mechanism for the inhibitor while acquired AAS analysis results revealed that the concentration of iron in the inhibited corrosive medium is less than the concentration of iron in the uninhibited solution after immersion with Ms at the same contact time and was also observed to reduce with upsurge in concentration of the inhibitor. SEM micrographs acquired revealed that the existence of the studied compound lessened the degree of corrosion in addition to decreased surface roughness signifying establishment of protective inhibitor film at the Ms surface. The energy of highest occupied molecular orbital (E_{HOMO}) as well as energy of lowest unoccupied molecular orbital (E_{LUMO}) remained estimated via density functional theory (DFT) method from which other parameters were determined. The results acquired from computational studies were in conformity with those from experimental studies and both validate the use of HL chelator as an excellent and efficient inhibitor for the corrosion of Ms in 1 M HCl.

KEYWORDS: *N*-(1,4-dihydro-1,4-dioxonaphthalene-3-yl) pyrazine-2-carboxamide, corrosion, DFT, adsorption, percentage inhibition.

INTRODUCTION

Acid solutions remain extensively adopted in manufacturing processes, with imperative grounds of usage comprising acid pickling of steel and iron, chemical washing plus minerals' fabrication in addition to oil well acidification. Amid acids adopted, the hydrochloric acid (HCl) employed for pickling of metallic species, acidification of oil wells plus cleaning of scales is less inexpensive, effectual as well as straightforward when likened to other acids (Shreir, 2010). This acid induces metallic dilapidation owing to its ferociousness (Saqalli1 *et al.,* 2017).

Corrosion of metals and their alloys induces colossal financial loss, particularly in petrochemical as well as oil and gas industries where acid solutions are ordinarily applied in countless operations (Fouda *et al.,* 2017a). As production plus engineering procedures gets multifaceted, the impacts arising from corrosion, safety risks plus disruptions in generating-plant actions also become expensive. Recently, interest in the regulation in addition to stoppage of corrosion has largely improved (Pierre, 2008) mostly with the usage of carbon-based compounds to avert or lessen corrosion of metallic exteriors. The usage of carbon-based compounds is extensively acknowledged essentially as frugally

Festus Chioma, Department of Chemistry, Ignatius Ajuru University of Education, P.M.B. 5047 Rumuolumeni, Port Harcourt, Rivers State, Nigeria
Odozi, Nnenna W., Physical Chemistry Unit, Department of Chemistry, University of Ibadan, Oyo State, Nigeria
Mchihi M. Moses, Physical Chemistry Unit, Department of Chemistry, University of Ibadan, Oyo State, Nigeria
Olatunde, M. Abimbola Physical Chemistry Unit, Department of Chemistry, University of Ibadan, Oyo State, Nigeria

feasible in contrast to other methodologies that are applied in the deterrence of corrosion (Lutendo *et al.,* 2017). Researchers opined that the inhibition effect of carbon-based compounds is principally reliant on their functional groups, steric influence, electronic density of donor atoms, orbital attractiveness of contributing electrons; while their inhibiting workability is largely clarified by the formation of adsorbed film on the metallic surfaces (Mahendra *et al.,* 2015; Odozi *et al.,* 2020). Most of the well acknowledged acid inhibitors are carbon-based compounds comprising N, S plus O atoms, and the adeptness of these compounds essentially depend on their capabilities to be adsorbed on the metallic surfaces with the polar groups acting as reactive centres (Louadi *et al.,* 2017). Although countless artificial compounds display worthy anticorrosive actions, most of them are extremely toxic to both humans as well as the environs, while some are frequently costly as well as non-biodegradable (Fouda *et al.,* 2017b). Therefore, there is need to investigate the inhibitory effect of compounds with desirable properties on the corrosion rate of steel in non-basic media. This study investigates the inhibitory effect of *HL chelator* on the corrosion of Ms in 1M HCl.

MATERIALS

All reagents; (pyrazine-2-carboxamide ($C_5H_5N_3O$), 2-hydroxy-1,4-naphthoquinone ($C_{10}H_6O_2$), undiluted ethanoic (CH_3COOH) and hydrochloric (HCl) acids, acetone (CH_3COCH_3), sodium hydroxide (NaOH), zinc-dust, triethylamine ($(C_2H_5)_3N$) and ethylenediamine ($(H_2NC_2H_2NH_2)$) were entirely supplied by Sigma-Aldrich limited while CH_3CH_2OH bought as container grade was distilled via known techniques (Mendham *et al.,* 2000; Odozi *et al.,* 2020). The Ms were obtained from Ken Johnson limited Uyo, Akwa Ibom State, Nigeria.

METHODS

The melting point temperature, FTIR, plus UV-VIS spectra as well as elemental content compositions of C H N of our prepared chelator-ligand were acquired according to Festus *et al.,* (2018). Additionally, ^{1}H and ^{13}C- NMR were employed for the analysis of the chelator (Festus *et al.,* 2019) which was also examined for solubility in polar plus non-polar solvents (Festus and Don-Lawson, 2018)

Experimental

Synthesis of HL Chelator Ligand

To equal-mole of $C_{10}H_6O_2$ (4.9 g; 0.02 mol), powdered $C_5H_5N_3O$ (3.4 g; 0.02 mol) in absolute methyl-alcohol (100 mL) was drop-wisely added and catalyzed with 8 drops of glacial acetic acid. The mixture was stirred and refluxed for 3 hrs, cooled, and the yellow solid filtered under suction, washed from ethyl-alcohol to acquire a bright yellow crystals in 64% yield (2.73 g) and melting point of 150-152^{o}C.

Weight loss measurements

The Ms specimens (Coupons) adopted for WL measurements were acquired from Ken Johnson limited Uyo, Akwa Ibom State and cut into 4×4cm dimensions. The Ms were washed comprehensively with purified H_2O as well as detergents and degreased with CH_3CH_2OH. The specimens were then rinsed using CH_3COCH_3, open-dried as well as weighed. The 1 M HCl solution was prepared by dilution of 35.4% HCl with purified H_2O. Five varied concentrations (1×10^{-5} M, 3×10^{-5} M, 5×10^{-5} M, 7×10^{-5} M, 9×10^{-5} M) of the inhibitor solutions were prepared. The prepared coupons (6 at a time) were immersed in six varied beakers comprising 100 mL of HCl and 100 mL each of five varied concentration of the inhibitor solution. The coupons were harvested after 5 hrs, dipped in zinc dust/NaOH solution, washed in soapy H_2O to do away with the corrosion product formed over the surface of coupon, degreased in CH_3CH_2OH, dipped in CH_3OCH_3 and dried after which the coupons were accurately weighed. The inhibitory effect of the chelator-ligand was monitored at five varied temperatures (303K, 313K, 323K, 333K, and 343K) with the aid of a thermostated H_2O bath (Abeng *et al.,* 2017). The WL, corrosion rate (CR), inhibition efficiency (%IE) plus the degree of superficial coverage (θ) of the appraised inhibitor on the surface of Ms remained calculated using the relationships in equations 1-4 (Eldesoky *et al.,* 2015).

$$WL = (W_o - W_1)/A \quad (1)$$

$$CR = (W_o - W_1)/At \quad (2)$$

$$\%IE = [(CR_{blank} - CR_{inh})/ CR_{blank}] \times 100 \quad (3)$$

$$\%IE = \theta \times 100 \quad (4)$$

AAS measurements

The concentration of iron (Fe) in 1M HCl medium with as well as without the inhibitor (varied concentrations) after immersion with Ms at the same contact time was determined using bulk 205 AAS.

SEM measurements

COATER MODEL Q150R ES SEM was adopted to evaluate the superficial morphological variations. The Ms Plates for this study remained thoroughly cleaned and immersed in 1M HCl medium in the presence as well as absence of inhibitor. After immersion, the coupons were scorned off to do away with the corrosion product formed over the surface, washed and dried for imaging.

Computational studies

The full optimization for the inhibitor molecule was acquired via DFT method as reported by Festus *et al.,* (2021). This is to aid in determining molecular properties defining the global reactivity of the inhibitor compound such as HOMO, LUMO, electronegativity (χ), the chemical potential (μ), fraction of transferred electrons (ΔN) plus global hardness (η). This choice is based on the fact that the DFT method has proven to be a very valuable methodology in investigating the inhibitor/superficial interface plus to evaluate investigational data (Saqalli1 *et al.,* 2017). Agreeing with Koopman's theorem, the HOMO energy is associated to the ionization potential (I) while LUMO energy is related to the electron affinity (A), as follows (Udhayakala, 2015).

$I = -E_{HOMO}$

$A = -E_{LUMO}$

The energy gap (ΔE) is determined as follows:

$\Delta E = E_{LUMO} - E_{HOMO}$

Then, the χ, the electrophility index, softness (σ) and η were appraised using the following relationships (Obi-Egbedi *et al.,* 2011).

$$\chi = \frac{I+A}{2} \quad \text{or} \quad \chi = -\frac{E_{LUMO}+E_{HOMO}}{2} \quad \text{.......... (5)}$$

$$\eta = \frac{I-A}{2} \quad \text{or} \quad \eta = -\frac{E_{LUMO}-E_{HOMO}}{2} \quad \text{.......... (6)}$$

$$\omega = \frac{\chi^2}{2\eta} \quad \text{................. (7)}$$

$$\sigma = \frac{1}{\eta} \quad \text{...................... (8)}$$

The fraction of transferred electrons (ΔN), in a reaction of two systems with varied electro-negativities in this specific situation, a metallic surface plus the inhibitor molecules, were determined following Pearson's theory (Saqalli1 et al., 2017; Mahendra *et al.,* 2015):

$$\Delta N = \frac{\chi_{Fe} - \chi_{inh}}{2(\eta_{Fe} + \eta_{inh})} \quad \text{......................(9)}$$

Where χ_{Fe} is theoretical value for the χ of bulk iron = 7 eV, χ_{inh} is the χ of inhibitor molecule, η_{Fe} is η of Fe=0 and η_{inh} is the η of the inhibitor molecule.

RESULTS AND DISCUSSION

Synthesis

The reaction of $C_{10}H_6O_2$ with $C_5H_5N_3O$ in CH_3CH_2OH solution gave a stable HL chelator ligand (Figure 1). All data obtained were corroborative of the suggested structure for the synthesized HL chelator-ligand. The compound remained extremely colored assuming a solid state.

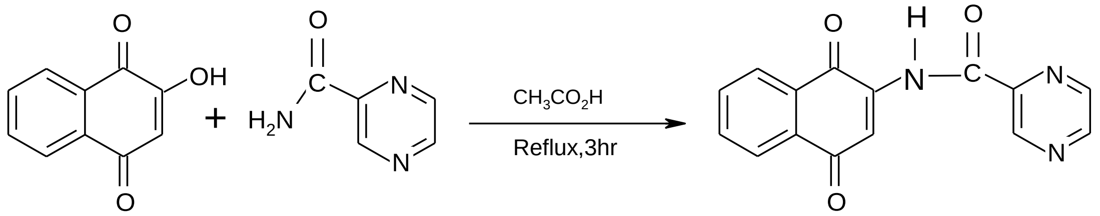

Figure 1: Synthetic Scheme for HL Chelator Ligand

Elemental and Solubility Analysis

The solubility tests of the ligand in both polar and non-polar organic solvents have been evaluated. Generally, the chelator exhibited varied solubilities in the solvents used but was majorly or slightly insoluble in H_2O and nitromethane. Additionally, the ligand had good solubilities in three solvents; chloroform, dimethylsulfoxide and dimethylformamide but were sparingly soluble in ethanol, methanol and dichloromethane. The analysis for the elemental composition conformed to a 1:1 stoichiometry for our synthesized chelator. The investigational values acquired remained strongly in conformity with hypothetical data as well as consistent with the chemical composition for the synthesized chelator.

FTIR, UV-Vis and NMR Studies

The substantial infrared spectral bands of the pyrazine-based chelator observed amid 350-4000 cm^{-1} remained cautiously apportioned by matching the spectra of the synthesised chelator with documented reports on comparable systems (Suparna, 2013; Festus *et al.,* 2018). The chelator displayed no bands conforming to amide moiety frequently detected in the spectrum of the amine adopted for synthesis, suggestive of condensation through the amide nitrogen with the naphthoquinone (Valarmathy and Subbalakshmi, 2014; Odozi *et al.,* 2020). The *v*(C=N) detected as a lone band within the ligand spectrum was indicative of Fermi resonance (Kalsi, 2004; Osowole and Festus, 2013). Likewise, the v(C=O) stretching band observed, remained a sharp band in the HL chelator at 1672 (Festus *et al.,* 2019), while sharp absorption bands at 1537-1579 cm^{-1}, 1366-1491 cm^{-1} and 981-991 cm^{-1} remained apportioned to *v*(C-N) of the aromatic rings, *v*(C-C) and *δ*(C-H) vibrations correspondingly. The chelator; HL presented bands at 26247-28653 cm^{-1} assigned to $n\rightarrow\pi*$ plus $\pi\rightarrow\pi*$ transition of the C-C, C=C, C=N plus C=O moieties (Osowole and Festus, 2015a, b). The HL chelator has been subjected to NMR (^1H and ^{13}C) studies. The $C_{10}H_6O_2$ protons (H_9, $H_{15,16}$ plus $H_{14,17}$) remained as lone signal at 6.52 ppm, twofold signals at 7.33 plus within 7.75-7.77 ppm separately. Also, cyclic hydrogen signals of the $C_5H_5N_3O$ fragment stood recognised as twofold signals at 6.06-6.12 ppm and threefold signals at 7.80-7.99 ppm for H_5 plus $H_{4,6}$ atoms. The signal due to O-H group typical of $C_{10}H_6O_2$ remained absent in the chelator spectrum, but a broad-like signal at 4.79 ppm distinctive of cyclic C-NH (s, N_7H) fragment was noticed. The N-H signal validates the suggested ketoamine tautomeric assemblage for the chelator. The ^{13}CNMR spectrum displayed resonance signals of the $C_{10}H_6O_2$ CO groups (C_{10}, C_{11}) at 181.5 ppm and 184.5 ppm. Moreover, detected resonance signals at 158.0 ppm, 125.4 ppm, 130.6 ppm, 125.9 ppm and 132.1 ppm remained accredited to C_8, C_9, $C_{12,13}$, $C_{14,17}$ plus $C_{15,16}$ atoms correspondingly of the $C_{10}H_6O_2$ moiety. Nonetheless, the resonance signals owing to C_2, C_5 plus $C_{4,6}$ of the $C_5H_5N_3O$ fragment were seen at 153.4 ppm, 110.8 ppm plus 133.1-134.5 ppm.

Weight loss

The impact of temperature on the corrosion inhibition of Ms in free acid and inhibited 1.0 M HCl remained studied at 303K, 313K, 323K, 333K and 343K. Table 1 shows corrosion rates (CR), %IE, θ and WL for Ms in blank solution and inhibited solutions at varied temperatures and concentrations. The result presented in Table 1 showed that the rate of corrosion of Ms declined with upsurge in the concentration of the inhibitor owing to the amplified quantity of inhibitor molecules adsorbed on the steel surface, hence affording wide superficial coverage (Loto *et al.,* 2013). Similarly, it may be deduced that the corrosion rate of Ms with as well as without the inhibitor solutions escalates with temperature. This is also exemplified in Figure 1. This finding can be rationalised by the fact that the improved impact of temperature on the dissolution process of Ms in non-basic media, increases the corrosion rate, and/or partial desorption of the inhibitor from the metallic surface, causing consequentially a decrease of the inhibitory efficiency (Saqalli1 *et al.,* 2017). Figure 2 denotes deviation of %IE with inhibitor concentration. The bars acquired designate continuous rise in %IE with increasing inhibitor concentration accompanied by a decrease in corrosion rate (Loto *et al.,* 2013). The %IE also increases with decrease in temperature. The superficial coverage data denote a continuous proliferation in film establishment with rise in inhibitor additionally heightens the IE (Loto *et al.,* 2013).

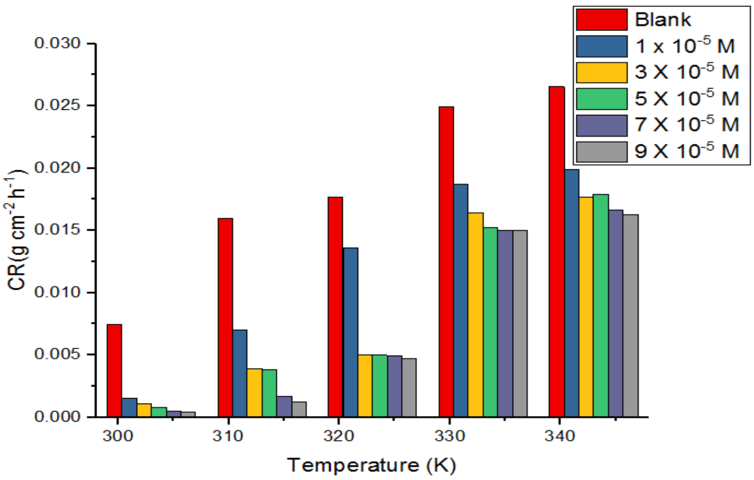

Figure 1: Variation of corrosion rate with temperature

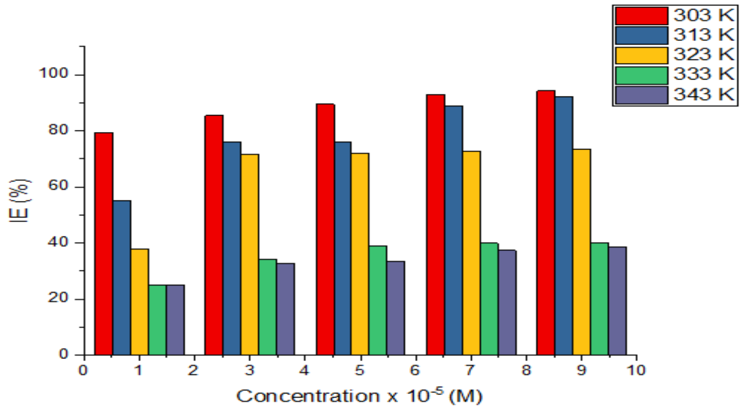

Figure 2: Variation of % IE with inhibitor concentration

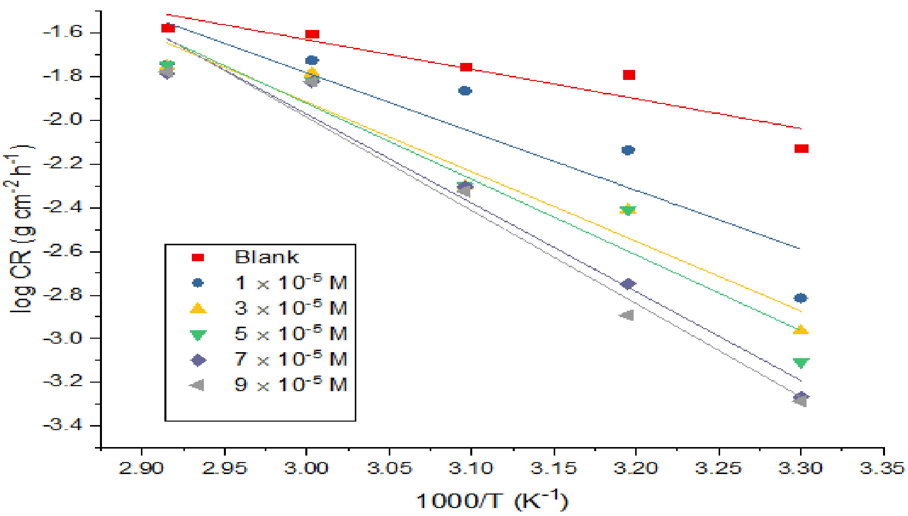

Figure 3: Arrhenius plots of log CR versus 1000/T for Ms in 1 M HCl solution at varied concentrations of the inhibitor

The activation energy (E_a) for dissolution of Ms in 1 M HCl solution was determined from Arrhenius plot. Arrhenius equation is stated thus (Abeng *et al.*, 2017):

$$\log \mathrm{CR} = -\frac{\mathrm{Ea}}{2.303\mathrm{RT}} + \log \mathrm{A} \quad \text{..} \quad (10)$$

Table 1: Corrosion parameters of Ms in 1.0 M HCl solution with as well as without the inhibitor at varied temperatures, acquired from WL measurements

Temperature (K)	Conc. (M)	CR ($gcm^{-2}h^{-1}$)	%IE	Θ	Wt loss
303	Blank	0.00746			0.0373
	1×10^{-5}	0.00153	79.49	0.7949	0.0077
	3×10^{-5}	0.00109	85.39	0.8539	0.0054
	5×10^{-5}	0.00078	89.54	0.8954	0.0027
	7×10^{-5}	0.00052	93.03	0.9303	0.0027
	9×10^{-5}	0.00043	94.24	0.9424	0.0025
313	Blank	0.01623			0.0811
	1×10^{-5}	0.00729	55.08	0.5508	0.0364
	3×10^{-5}	0.00391	75.91	0.7591	0.0195
	5×10^{-5}	0.00389	76.06	0.7606	0.0194
	7×10^{-5}	0.00178	89.03	0.8903	0.0089
	9×10^{-5}	0.00128	92.11	0.9211	0.0064
323	Blank	0.01768			0.0884
	1×10^{-5}	0.011	37.78	0.3778	0.0681
	3×10^{-5}	0.005	71.72	0.7172	0.025
	5×10^{-5}	0.00495	72	0.72	0.0249
	7×10^{-5}	0.00499	72.77	0.7277	0.0248
	9×10^{-5}	0.00472	73.3	0.733	0.0236
333	Blank	0.02494			0.1247
	1×10^{-5}	0.01874	24.86	0.2486	0.0937
	3×10^{-5}	0.01643	34.12	0.3412	0.0822
	5×10^{-5}	0.01521	39.01	0.3901	0.0761
	7×10^{-5}	0.015	39.86	0.3986	0.075
	9×10^{-5}	0.01499	39.9	0.399	0.0749
343	Blank	0.02654			0.1327
	1×10^{-5}	0.01989	25.06	0.2506	0.0894
	3×10^{-5}	0.01789	32.59	0.3259	0.0885
	5×10^{-5}	0.0177	33.31	0.3331	0.0895
	7×10^{-5}	0.01665	37.26	0.3726	0.0814
	9×10^{-5}	0.01628	38.66	0.3866	0.0834

A plot of log CR versus 1/T for the corrosion of Ms in 1 M HCl with as well as without the varied concentrations of inhibitor is represented in Figure 3. The data of Ea remained apprised from the slope ($-E_a/2.303R$) of the graph plus the results presented in Table 2. The higher data of E_a with the inhibitor as likened to the Ea without the inhibitor in 1 M HCl solution denotes that the inhibitor has an effect on the Ea for the corrosion led to decrease of corrosion rate of Ms in the presence of inhibitor.

Table 2 Values of Ea acquired from Arrhenius plot for Ms in 1.0 M HCl solution with as well as without the inhibitor.

Concentration ($\times 10^{-5}$ M)	E_a (kJ/mol)
Blank	7.077
1	14.051
3	16.648
5	18.100
7	21.214
9	22.277

Almost straight lines were acquired by plotting C/θ Vs C as presented in figure 4, which substantiates that the adsorption of this compound obeys Langmuir isotherm best among other isotherms.

$$\frac{C}{\theta} = C + \frac{1}{Kads} \qquad \text{...(11)}$$

Adsorption parameters calculated from LAI for Ms in 1.0 M HCl solution at a temperature range of 303-343K are shown in Table 3. The slight nonconformity of the slopes from normal could be apportioned to the molecular interface amid adsorbed inhibitor species, a non-considered factor during the derivation of the Langmuir equation. The Langmuir isotherm adopts that:

a) The metallic superficial consist of a known amount of adsorption spots plus each position having an adsorbate

b) ΔG_{ads} remains similar for all chelate points in addition to been non-dependent of θ

c) The adsorbates do not interface with one another implying existence of no lateral interaction effect of adsorbates on ΔG_{ads} [21].

The change in free energies of adsorption was determined from the equilibrium constant of adsorption adopting the expression: $\Delta G_{ads} = -RT \ln (55.5 \times K_{ads})$ ………………… (12)

The value 55.5 remains the concentration (mol/L) of H_2O in solution (Manimegalai and Manjula, 2015). The negative value of ΔG_{ads} denotes that the adsorption of inhibitor molecules on the metallic surface is spontaneous (Mahendra *et al.,* 2015). Largely, values of ΔG_{ads} upto -20 kJ/mol are compatible with physisorption (i.e electrostatic interaction amid the charged molecules plus charged metal); those around -40kJ/mol or more negative than -40kJ/mol are compatible with chemisorption (charge distribution or transmission from carbon-based molecules to metallic surface to form a coordinate type of bond) (Mahendra *et al.,* 2015; Loto *et al.,* 2013). The dada of ΔG_{ads} acquired denoted that the adsorption mechanism of the inhibitor molecules on the metallic surface is largely chemisorption since values of ΔG_{ads} determined at four (4) varied temperatures fall within the limit of chemisorption.

Table 3 Adsorption parameters calculated from LAI for Ms in 1.0 M HCl solution at a temperature range of 303-343K

Temperature (K)	Slope	Intercept ($\times 10^{-5}$)	Correlation coefficient (R^2)	K_{ads} ($\times 10^5$ M^{-1})	ΔG (KJ/mol)
303	1.04305	0.29955	0.99934	3.33834100	-42.16
313	0.98951	1.04150	0.98515	0.96015360	-40.30
323	1.06925	2.15475	0.91249	0.46409096	-39.64
333	2.29248	1.68906	0.99840	1.35725000	-43.84
343	2.28560	2.47240	0.75804	0.9244458	-44.06

Thermodynamic parameters (alteration in enthalpy plus alteration in entropy) were determined via the transition state equation (equation 13)

$$CR = \frac{RT}{Nh} \exp\left(\frac{\Delta S}{R}\right) \exp\left(-\frac{\Delta H}{RT}\right) \quad \text{………………………………………………………….(13)}$$

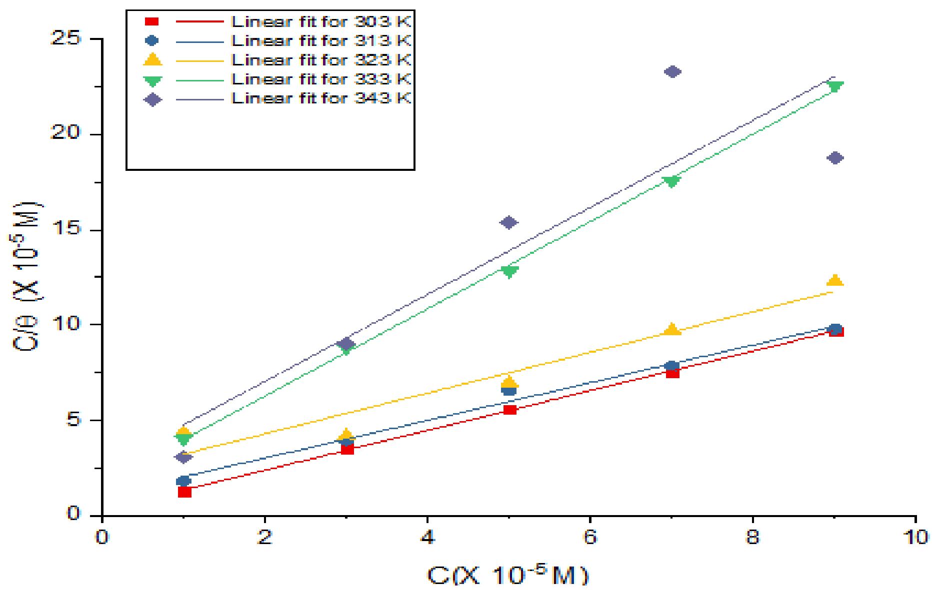

Figure 4: Langmuir plots for the adsorption of HL molecule on the surface of Ms at 303K, 313K, 323K, 333K and 343K

A plot of log (CR/T) versus 1/T **(**Figure 5) provided straight lines similar to the Arrhenius plot with slope of –ΔH/2. 303R plus intercept of log [log(R/Nh) + (ΔS/2.303R)], from which the thermodynamic parameters remained determined. The evaluated values of ΔH plus ΔS acquired from this plot are also given in Table 4. The positive values of ΔH both with as well as without the inhibitor reflect the endothermic nature of the Ms dissolution process (Ekemini *et al.,* 2017). The negative values of ΔS both with as well as without the inhibitor denotes that the development of an active compound in the rate determining step signifies an integration and not a dissociation step, denoting a decline in disorder which occurs in the process of transition from precursors to the activated phase (Mahendra *et al.,* 2015).

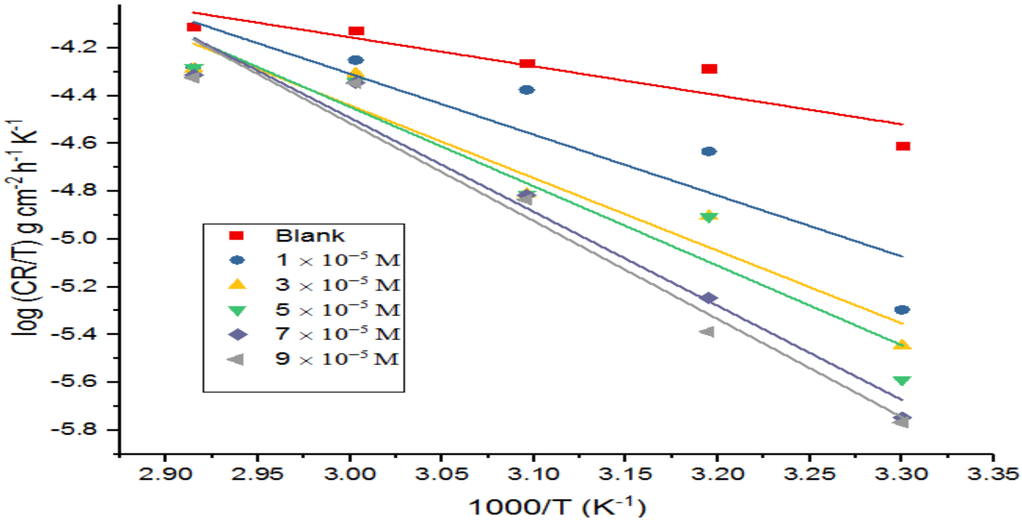

Figure 5: Transition state plots of log (CR/T) versus 1000/T for Ms in 1 M HCl solution at varied concentrations of the inhibitor

Table 4 Change in Enthalpy and entropy values acquired from Transition state plot for Ms in 1.0 M HCl solution with as well as without the inhibitor

Concentration (x 10^{-5} M)	ΔH (kJ/mol)	ΔS (J/mol/K)
Blank	6.350	-207.333
1	13.32	-133.666
3	15.935	-107.751
5	17.387	-91.638
7	20.575	-57.482
9	21.444	-49.885

AAS Studies

The result acquired from AAS analysis revealed that the concentration of iron in the inhibited corrosive medium is less than the concentration of iron in the uninhibited solution (blank) after immersion with steel at the same contact time. This denotes that the presence of the inhibitor actually reduced the corrosion of the metal as earlier deduced from WL measurements. It can also be observed from table 5 that the concentration of iron in the inhibited solutions decreases with upsurge in concentration of the inhibitor

Table 5 concentration of iron (Fe) in uninhibited and inhibited solution determined by AAS analysis after immersion with steel

Concentration of inhibitor solution (M)	Concentration of Iron, Fe (ppm)
Blank	4.471
1 x 10^{-5}	4.074
7 x 10^{-5}	0.649
9 x 10^{-5}	0.632

SEM

SEM photomicrographs for Ms only and Ms in 1 M HCl solution with as well as without the inhibitor are shown in Figure 6. Based on the results, it could be clearly detected that the superficial part of Ms specimen appears to be actually even indicating no corrosion whereas the surface of Ms specimen dipped in 1 M HCl solution without the inhibitor on the other hand is precisely uneven with the surface dented owing to metallic dissolution. Nevertheless, with the inhibitor ($5x10^{-5}$M) decreased the rate of corrosion with superficial mutilation lessened significantly when likened to the photomicrographs of Ms dipped in acidic medium without the inhibitor, signifying establishment of shielding inhibitor film at the Ms surface (Mahendra *et al.,* 2015)

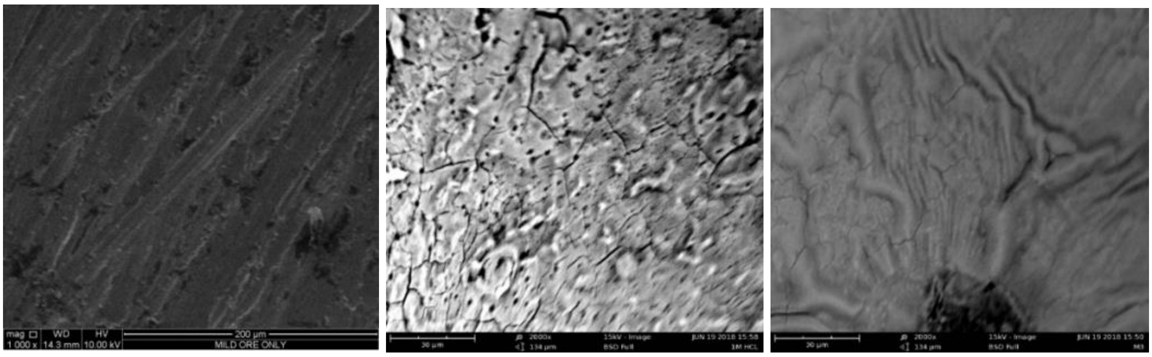

Figure 6: SEM photomicrographs (a) Ms only (b) Ms immersed in 1M HCl (c) Ms in inhibited corrosive medium

Computational studies

The high value of E_{HOMO} as shown in Table 6 denote greater tendency of donating electrons in addition, this denotes an improved inhibitory action via amassed adsorption of the inhibitor on a metallic surface, while low value of E_{LUMO} denotes electron accepting potential of the molecule (that is, the adsorption capability of the inhibitor to the metallic superficial proliferates with an increase of E_{HOMO} as well as decrease of E_{LUMO}) (Rodi and Baba, 2016; Festus *et al.,* 2020). The Optimized molecular structures**,** HOMO, LUMO plus electrostatic potential map images are presented in figure

Table 6 Quantum chemical descriptors of the appraised inhibitor

Parameters	
E_{HOMO} (eV)	-6.84
E_{LUMO} (eV)	-3.24
ΔE (eV)	3.60
I (eV)	6.84
A (eV)	3.24
η (eV)	1.80
σ (eV^{-1})	0.55
ω (eV)	7.06
Fractions of electron transferred ΔN	0.54
χ (eV)	5.04
Dipole moment μ (Debye)	2.04
$\Delta E_{Back\text{-}donation}$	-0.45

Largely, ΔN shows IE arising from relocation of electrons on the inhibitor to the iron specie (Mahendra *et al.,* 2015). When ΔN value is lower than 3.6, proficiency of inhibition proliferates with amassing electron-donating capability of the inhibitor at the metallic surface (Mahendra *et al.,* 2015). The varied acquired data of the electrostatic ability remain denoted by varied shades; red signifies the portions of the utmost non-positive electrostatic capabilities, blue signifies the sections of the maximum non-negative electrostatic ability and green signifies the state of zero potential. Figure 7d affords a pictorial depiction of the chemically active spots as well as relative reactivity of atoms and it is clear that oxygen atom (red region) is most likely to react with electrophilic sites while hydrogen atoms (blue region) are most likely to react with nucleophilic sites (Bendjeddou *et al.,* 2016).

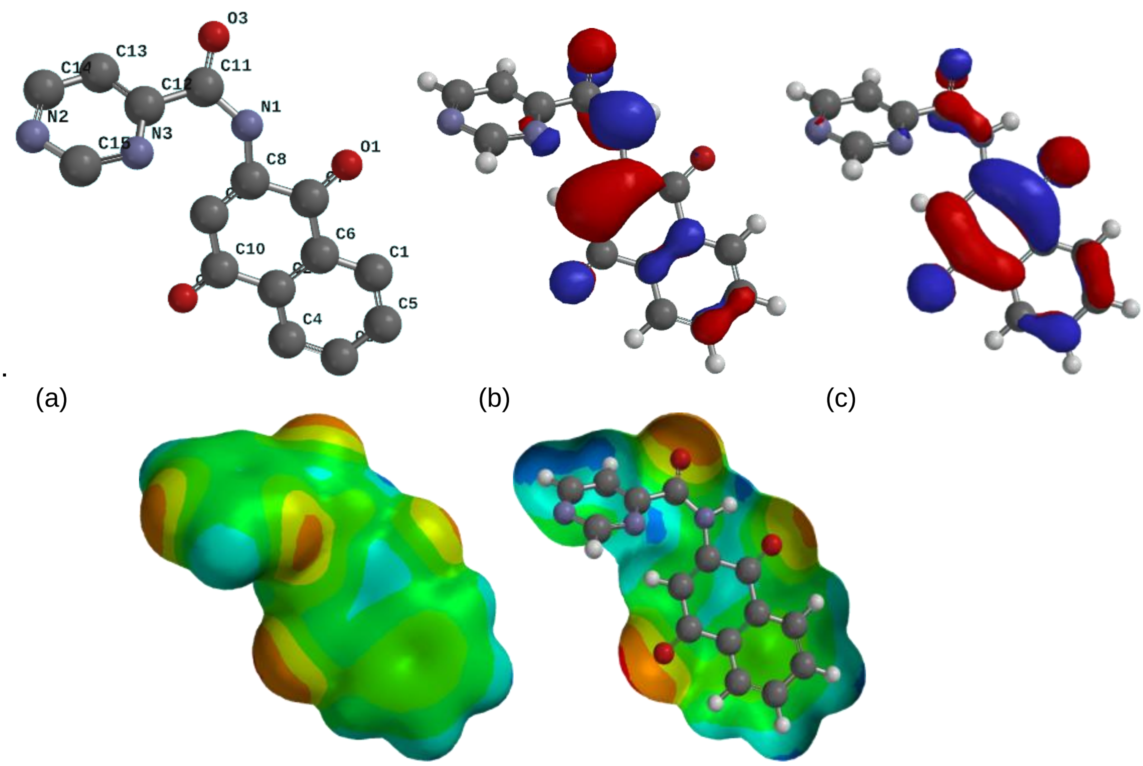

(a) (b) (c)

(d)

Figure 7: (a) The Optimized molecular structures of the studied compound (b) HOMO (c) LUMO (d) Electrostatic potential map

The Mulliken charge distributions of the synthesised compound are obtainable in Table 7. The table denotes that all the oxygen and nitrogen species had high negative charge densities indicating that the most likely reactive position(s) for the adsorption of these inhibitors on Ms surface is situated on these atoms (Mao, 2014).

Table 7 Ground-State Mulliken Net Atomic Charges

Atom	Atomic charge (a.u)
1 C	-.168877
2 C	.049469
3 C	-.120351
4 C	-.176536
5 C	-.127402
6 C	.053295
7 C	.348575
8 C	.363005
9 C	-.230366
10 C	.399985
11 O	-.485604
12 O	-.483059
13 N	-.724714
14 C	.561983
15 O	-.457578
16 C	.221472
17 N	-.372366
18 N	-.429353
19 C	-.139093
20 C	.050757
21 C	.173644
22 H	.171004
23 H	.149965
24 H	.172768
25 H	.149339
26 H	.160890
27 H	.371551
28 H	.181167
29 H	.166712
30 H	.169718

CONCLUSION

The inhibitory effect of *HL chelator*on the corrosion rate of Ms in 1.0 M HCl solution has been appraised using WL measurements, atomic absorption spectrophotometry, scanning electron microscopy and computational studies. The results acquired from experimental studies denote that our synthesised compound displays excellent performance as inhibitor for Ms corrosion in 1.0 M HCl solution since corrosion rate was noticed to decline with the appraised compound and its IE increased with concentration. The result of parameters (ΔE, χ, η, σ, ω, plus ΔN) from inhibitor molecule to the metallic surface determined from E_{HOMO} and E_{LUMO} to correlate the calculated structural and electronic parameters of the appraised inhibitor with its corrosion IE denote a good conformity amid experimental and computational studies hence further validates the potency of the studied compound as inhibitor for Ms corrosion in 1.0 M HCl solution.

REFERENCES

Abeng, F. E., Idim, V. D., Obono, O. E. and Magu, T. O., 2017. Adsorption and adsorption isotherm: application to corrosion inhibition studies of mild steel in 2 M HCl. World Scientific News. 77(2): 298-313.

Bendjeddou, A., Abbaz, T., Gouasmia, A. K. and Villemin, D., 2016. Molecular Structure, HOMO LUMO, MEP and Fukui Function Analysis of Some TTF- donor Substituted Molecules Using DFT (B3LYP) Calculations. International Research Journal of Pure and Applied Chemistry 12.1):1-9.

Ekemini, I., Onyewuchi, A. and Abosede, J., 2017. Evaluation of Performance of Corrosion Inhibitors Using Adsorption Isotherm Models: An Overview. Chemical Science International Journal. 18(1): 1-34.

Eldesoky, A. M, Dia, A. M, and El-Bindary, A. A., 2015. Some antipyrine derivatives as corrosion inhibitors for copper in acidic medium: Experimental and quantum chemical molecular dynamics approach. Journal of Material and Environmental Sciences 6(8): 2148-2165.

Festus, C., Okafor S. N. and Ekennia A. C., 2019. Heteroleptic Metal Complexes of a Pyrimidinyl Based Schiff Base Ligand Incorporating 2,2′ -Bipyridine Moiety: Synthesis, Characterization, and Biological Studies. Front. Chem. 7(862); 1-12. doi: 10.3389/fchem.2019.00862.

Festus, C., Ekennia, A. C., Osowole, A. A., Olasunkanmi, L. O., Onwudiwe, D. C. and Ujam, O. T., 2018. Synthesis, experimental and theoretical characterization and antimicrobial studies of some Fe(II), Co(II) and Ni(II) complexes of 2-(4,6-dihydroxypyrimidin-2-ylamino) naphthalene-1,4-dione. Research on Chemical Intermediates 44(10):5857-5877.

Festus, C. and Don-Lawson, C. D., 2018. Synthesis, spectral, magnetic and in-vitro biological studies of organic ligands and their corresponding heteroleptic divalent d-metal complexes. The Pharmaceutical and Chemical Journal; 5(3):118-129. www.tpcj.org

Festus, C., Okafor, S. N. and Ekennia, A. C., 2019. Heteroleptic Metal Complexes of a Pyrimidinyl Based Schiff Base Ligand Incorporating 2,2′ -Bipyridine Moiety: Synthesis, Characterization, and Biological Studies. Front. Chem. 7(862): 1-12.

Festus, C., Odozi, W. N. and Olakunle, M., 2020. Preparation, Spectral Characterization and Corrosion Inhibition Studies of (E)-N-{(Thiophene- 2yl)methylene}pyrazine-2-carboxamide Schiff Base Ligand. Protection of Metals and Physical Chemistry of Surfaces, 56(3): 651–662.

Festus, C., Jude, I. A., Collins, U. I., 2021. Ligation Actions of 2-(3-hydroxypyridin-2-ylamino) naphthalen-1,4-dione: Synthesis, Characterization, In-vitro Antimicrobial Screening, and Computational Studies. Indian Journal of Heterocyclic Chemistry, 31(01); 1-13.

Fouda, A. S., Diab, M. A, and Fathy, S., 2017a. Role of Some Organic Compounds as Corrosion Inhibitors for 316L Stainless Steel in 1 M HCl. International Journal of Electrochemical Science 12. 347 – 362.

Fouda, A. S., Ismail, M. A., Abousalem, A. S. and Elewady, G. Y., 2017b. Experimental and theoretical studies on corrosion inhibition of 4-amidinophenyl-2,20-bifuran and its analogues in acidic media. Royal society of chemistry 7. 46414 -46430.

Kalsi, P. S., 2004. Spectroscopy of organic compounds. 6th Edition. New age International publishers: India 71-7249.

Loto, R. T., Loto, C. A. and Popoola, A. P., 2013. Effect of Aminobenzene concentrations on the corrosion inhibition of Mild Steel in sulphuric acid. International Journal of Electrochemical Science 7. 7016–7032.

Louadi, Y. E., Abrigach, F. and Bouyanzer, A., 2017. Theoretical and Experimental studies on the corrosion inhibition potentials of two tetrakis pyrazole derivatives for mild steel in 1.0 M HCl. Portugaliae Electrochimica Acta 35.3: 159-178.

Lutendo, C. M., Kabanda, M. M. and Ebenso, E. E., 2017. Experimental and theoretical studies on the corrosion inhibition of mild steel by some sulphonamides in aqueous HCl. Royal society of chemistry 1-38.

Mahendra, Y., Kumar, S. and Kumari, N. 2015. Experimental and theoretical studies on corrosion inhibition effect of synthesized Benzothiazole derivatives on mild steel in 15% HCl solution. International journal of electrochemical science 10. 602-624.

Manimegalai, S. and Manjula, P., 2015. Thermodynamic and Adsorption studies for corrosion Inhibition of Mild steel in Aqueous Media by Sargasam swartzii (Brownnalgae).Journal of Material and Environmental Sciences 6 (6): 1629-1637.

Mao, X. J., 2014. Atomic Charges in Molecules: A Classical Concept in Modern Computational Chemistry. Journal of Postdoctoral Research 2(2):15-18.

Mendham, J., Denney, R. C., Barnes, J., and Thomas, M., Vogel's Textbook of Quantitative Chemical Analysis, New Delhi: Pearson Education Ltd., 2000.

Obi-Egbedi, N. O., Obot, I. B., El-khaiary, M. I., Umoren, S. A. and Ebenso, E. E., 2011. Computational Simulation and Statistical Analysis on the Relationship Between Corrosion Inhibition Efficiency and Molecular Structure of Some Phenanthroline Derivatives on Mild Steel Surface. International Journal of Electrochemical Science 6. 5649 – 5675.

Odozi, N. W., Festus, C. and Dagoli, M. A., 2020. Synthesis, adsorption and inhibition behaviour of 2-[(thiophen-2-ylmethylidene)amino]pyridine-3-ol on mild steel corrosion in aggressive acidic media. Nigerian Research Journal of Chemical Sciences. 8(2):291-307.

Osowole, A. A. and Festus, C., 2013. Synthesis, characterization and antibacterial activities of some metal(II) complexes of 3-(-1-(2-pyrimidinylimino) methyl-2-napthol. Elixir Appl. Chem. 59 (2013) 15843-15847.

Osowole, A. A. and Festus, C., 2015a. Synthesis, spectral magnetic and antibacterial studies of some divalent metal complexes of 3-{[(4,6-dihydroxy pyrimidin-2- yl) Imino] methyl} Napthalen-2-ol. Journal of Chemical, Biological and physical sciences, **6**(11).

Osowole, A. A. and Festus, C., 2015b. Synthesis, characterization, antibacterial and antioxidant activities of some heteroleptic Metal(II) complexes of 3-{[-(pyrimidin-2- yl) imino]methyl}napthalen-2-ol. J. of Chemical, Biological and Physical Sciences. 6(1); 080-089.

Pierre, R. R., 2008. Corrosion Engineering Principles and Practice. McGraw-Hill Companies. United States of America. Chapter 2:19-32.

Rodi, Y. K. and Baba, Y., 2016. 2-oxo-N'-phenyl-1,2-dihydroquinoline-4-carbohydrazide as Corrosion Inhibitor for Mild Steel in Acidic Medium: Experimental Studies. Der Pharma Chemica 8(4): 159-169.

Saqalli1, L., Galai M., Benhiba, N. and Gharda, N., 2017. Experimental and theoretical studies of Alizarin as corrosion inhibitor for mild steel in 1.0 molar HCl solution. Journal of Materials and Environmental Sciences 8.7: 2455-2467.

Shreir, L. L., 2010. Basic concepts of corrosion . Elsevier B.V 1. 1–15.

Suparna, G., 2013. Synthesis and pharmacological studies of some bivalent metal complexes with Schiff based ligand derived from xipamide. Der Pharma Chemica 5(3): 232-235.

Udhayakala, P., 2015. Quantum chemical studies on the inhibition potentials of thiophene derivatives for the corrosion inhibitors of carbon steel. Journal of Chemical and Pharmaceutical Research 7(1): 803-810.

Valarmathy, G. and Subbalakshmi, R., 2014. Synthesis, spectral characterisation, electrochemical, and fluorescence studies of biologically active novel Schiff base complexes derived from E-4-(2-hydroxy-3-methoxybenzlideneamino)-N-(pyrimidin-2-yl) benzenesulfonamide. Turkish Journal of Chemistry 38: 521-530